Coexistence of toroidal and polar domains in ferroelectric systems: A strategy for switching ferroelectric vortex

Article *in* Journal of Applied Physics · June 2014

DOI: 10.1063/1.4881530

CITATIONS
7

READS
62

4 authors, including:

W. J. Chen
Sun Yat-Sen University
39 PUBLICATIONS **210** CITATIONS
SEE PROFILE

J. Y. Liu
Sun Yat-Sen University
6 PUBLICATIONS **35** CITATIONS
SEE PROFILE

Coexistence of toroidal and polar domains in ferroelectric systems: A strategy for switching ferroelectric vortex

W. J. Chen, Yue Zheng, Biao Wang, and J. Y. Liu

Citation: Journal of Applied Physics **115**, 214106 (2014); doi: 10.1063/1.4881530
View online: http://dx.doi.org/10.1063/1.4881530
View Table of Contents: http://scitation.aip.org/content/aip/journal/jap/115/21?ver=pdfcov
Published by the AIP Publishing

Coexistence of toroidal and polar domains in ferroelectric systems: A strategy for switching ferroelectric vortex

W. J. Chen,[1,2] Yue Zheng,[1,2,a)] Biao Wang,[1,b)] and J. Y. Liu[1,2]
[1]*State Key Laboratory of Optoelectronic Materials and Technologies, Sun Yat-sen University, 510275 Guangzhou, China*
[2]*Micro & Nano Physics and Mechanics Research Laboratory, School of Physics and Engineering, Sun Yat-sen University, 510275 Guangzhou, China*

(Received 14 April 2014; accepted 22 May 2014; published online 4 June 2014)

Phase field simulations have been conducted to investigate the vortex domain structure in ferroelectric nanodots epitaxially grown on ferroelectric nanofilm. It is found that the nanodot region has great impact on the domain evolution of the whole system. At suitable conditions (e.g., geometry, size, temperature, external strain, and electric field), the nanodot adopts a vortex domain pattern while the nanofilm maintains a polar domain. Interestingly, the vortex domain pattern of the nanodot can be switched by controlling the direction of the adjacent polar domain. Our study indicates an alternative strategy for controlling the chirality of vortex domain structure in nano-ferroelectrics. © *2014 AIP Publishing LLC*. [http://dx.doi.org/10.1063/1.4881530]

I. INTRODUCTION

Low-dimensional ferroelectric nanostructures are now drawing a large amount of attentions for their novel property of exhibiting a special type of domain structure with closure of polarization, namely, vortex domain structure (VDS).[1–5] As a new kind of polarization ordering, ferroelectric VDS exhibits distinct characteristics from the conventional domain structures and indicates wonderful applications in the field of domain and domain wall engineering.[6–8] One well-known potential application of ferroelectric VDS is the development of ultrahigh-density memory devices utilizing nanoscale vortices to carry information. Moreover, as a direct consequence of the truncated long-range interactions at the surfaces, ferroelectric VDS can be strongly affected by boundary conditions, external fields, as well as the system's size and geometry.[6,9–20] This further provides us promising mechanisms of achieving large and unusual properties basing on the control of VDS and indicates important applications such as developing novel sensors and actuators.

It is a natural idea to utilizing the vortex chirality to store information. However, the switching problem of ferroelectric VDS is so far not easy to solve, due to the fact that the toroidal moment of a ferroelectric vortex is conjugated to a curled electric field rather than a conventional electrostatic field.[7,14] The necessary switching curled electric field is generally large and highly localized, which is difficult to realize in practice. In literature, in order to gain regular control on ferroelectric VDS, both the effects of electrical and mechanical loads on VDS have been theoretically studied.[9–18] Using the first-principle-based effective Hamiltonian method, people have revealed the cooperative response of ferroelectric nanostructures to various types of electric fields (e.g., homogenous and inhomogeneous ones).[9–14] Particularly, Prosandeev and his coworkers proposed that vortex orientation could be controlled by inhomogeneous electrostatic field generated by charged tips near the ferroelectric nanodots.[10] They also showed that homogenous electrostatic field can be applied to switch the VDS in asymmetric ferroelectric rings[12] or rectangular systems with double vortices.[13] The VDS switching characteristics in ferroelectric nanostructure under a curled electric field has also been simulated by phase field model.[15] More recently, the effect of mechanical loads on VDS in various ferroelectric nanostructures has been investigated and novel VDS transformations have been revealed.[16–18] Summarizing these works, we notice that ferroelectric VDS switching may be achieved by electrostatic fields but with specific requirements on distribution of electrostatic field or the domain pattern. Meanwhile, it is possible to induce vortex multiplication, annihilation, or rotation rather than switching by mechanical loads. Nevertheless, most of the reported strategies are still difficult to realize by the current experimental techniques.

In this paper, we propose that ferroelectric vortex switching may be achieved by exploiting the coupling between the vortex domain pattern and adjacent polar domain in systems where the two types of domains can coexist. To demonstrate this idea, we take perovskite ferroelectric nanofilms with epitaxially grown nanodots (namely, nanofilm-dot systems) as our model systems (Fig. 1(a)). It is expected that there would be a coupling between the domains of the two regions across the coherent interface. Phase field simulations will be conducted to simulate the domain structure with taking into account the effects of geometry, size, temperature, and misfit strain. The first aim of this paper is to explore whether the nanofilm-dot systems can exhibit VDS in the nanodot with an adjacent polar domain in the nanofilm (Fig. 1(a)). The second aim is to show how the VDS in the nanodot can be switched by controlling adjacent polar domain in the nanofilm (Fig. 1(b)). Our study should be instructive for the control of VDS in ferroelectric nanostructures.

[a)]Author to whom correspondence should be addressed. Electronic address: zhengy35@mail.sysu.edu.cn
[b)]Electronic address: wangbiao@mail.sysu.edu.cn

II. THE PHYSICAL MODEL

In the phase field model, we choose the spontaneous polarization $\mathbf{P}=(P_1, P_2, P_3)$ as the order parameter. The electric displacement field $\mathbf{D}$ is expressed as $\mathbf{D}=\boldsymbol{\varepsilon}_\mathbf{b}\mathbf{E}+\mathbf{P}$, with $\mathbf{E}$ being the electric field and $\boldsymbol{\varepsilon}_\mathbf{b}$ being the background dielectric constant tensor.[21,22] Since the background material is the cubic paraelectric phase, the background dielectric constants in three axis directions are the same, i.e., $\varepsilon_b = \varepsilon_{11b} = \varepsilon_{22b} = \varepsilon_{33b}$. To take into account effects of the mechanical strain, electric field and surface, the total free energy of the ferroelectric system is written as a sum of the bulk Landau energy, elastic energy, gradient energy, electrostatic energy, and surface energy, i.e.,

$$F=\int_V (f_{\text{Land}}+f_{\text{elas}}+f_{\text{grad}}+f_{\text{elec}})dV+\int_S f_{\text{surf}}dS, \quad (1)$$

where V and S are the volume and surface of the ferroelectric system, respectively.

According to previous works, the Landau energy density is written as a six-order polynomial of the spontaneous polarization, i.e.,[23,24]

$$\begin{aligned} f_{\text{Land}} =& a_1(P_1^2+P_2^2+P_3^2)+a_{11}(P_1^4+P_2^4+P_3^4)\\ &+a_{12}(P_1^2P_2^2+P_1^2P_3^2+P_2^2P_3^2)\\ &+a_{111}(P_1^6+P_2^6+P_3^6)+a_{123}P_1^2P_2^2P_3^2\\ &+a_{112}\left[P_1^4(P_2^2+P_3^2)+P_2^4(P_1^2+P_3^2)+P_3^4(P_1^2+P_2^2)\right], \end{aligned} \quad (2)$$

where $a_1 \equiv (T-T_{c0})/(2\varepsilon_0 C_0)$ is the dielectric stiffness, with T_{c0} and C_0 being the Curie-Weiss temperature and Curie-Weiss constant of the bulk material, respectively, and ε_0 being the dielectric constant of vacuum. a_{ij} and a_{ijk} are the higher-order stiffness coefficients.

Under the condition of applied mechanical strain, the mechanical strain field (applied and internal) and its coupling with polarization contribute to the elastic energy density, which is described by

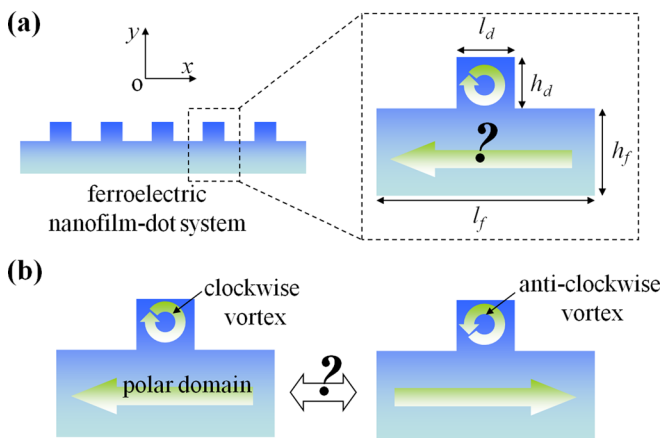

FIG. 1. Schematics of (a) a ferroelectric nanofilm-dot system and (b) the idea of switching vortex domain pattern in the nanodot by reversing the polar domain in the nanofilm.

$$\begin{aligned} f_{\text{elas}} =& \frac{1}{2}c_{ijkl}e_{ij}e_{kl}=\frac{1}{2}c_{ijkl}(\varepsilon_{ij}-\varepsilon_{ij}^0)(\varepsilon_{kl}-\varepsilon_{kl}^0)\\ =& \frac{1}{2}C_{11}\left[(\varepsilon_{11}-\varepsilon_{11}^0)^2+(\varepsilon_{22}-\varepsilon_{22}^0)^2+(\varepsilon_{33}-\varepsilon_{33}^0)^2\right]\\ &+C_{12}\left[(\varepsilon_{11}-\varepsilon_{11}^0)(\varepsilon_{22}-\varepsilon_{22}^0)+(\varepsilon_{11}-\varepsilon_{11}^0)(\varepsilon_{33}-\varepsilon_{33}^0)\right.\\ &\left.+(\varepsilon_{22}-\varepsilon_{22}^0)(\varepsilon_{33}-\varepsilon_{33}^0)\right]\\ &+\frac{1}{2}C_{44}\left[(\varepsilon_{12}-\varepsilon_{12}^0)^2+(\varepsilon_{13}-\varepsilon_{13}^0)^2+(\varepsilon_{23}-\varepsilon_{23}^0)^2\right], \end{aligned} \quad (3)$$

where c_{ijkl} and C_{ij} and are the fourth-rank and reduced elastic stiffness coefficients, respectively, and e_{ij}, ε_{ij}^0 and ε_{ij} are the components of elastic strain, eigenstrain total strain, respectively. The eigenstrain is related to the polarization as $\varepsilon_{ij}^0 = Q_{ijkl}P_kP_l$, with Q_{ijkl} being the fourth-rank electrostrictive coefficients. The strain field is determined by the mechanical equilibrium equation, i.e., $\sigma_{ij,j}=0$, where $\sigma_{ij}=c_{ijkl}e_{kl}$ is the stress components.

Moreover, the spatial polarization variation would contribute a gradient energy. To the lowest order of the Taylor expansion, the gradient energy density takes the form as

$$\begin{aligned} f_{\text{grad}} =& \frac{1}{2}G_{11}(P_{1,1}^2+P_{2,2}^2+P_{3,3}^2)\\ &+G_{12}(P_{1,1}P_{2,2}+P_{2,2}P_{3,3}+P_{1,1}P_{3,3})\\ &+\frac{1}{2}G_{44}\left[(P_{1,2}+P_{2,1})^2+(P_{2,3}+P_{3,2})^2+(P_{1,3}+P_{3,1})^2\right]\\ &+\frac{1}{2}G_{44}^{'}\left[(P_{1,2}-P_{2,1})^2+(P_{2,3}-P_{3,2})^2+(P_{1,3}-P_{3,1})^2\right] \end{aligned} \quad (4)$$

for ferroelectrics with a cubic paraelectric phase, with G_{11}, G_{12}, G_{44}, and $G_{44}^{'}$ being the reduced gradient energy coefficients.

According to previous works,[21,25] the electric energy density of a given polarization distribution is written as

$$f_{\text{elec}} = -(P_1E_1+P_2E_2+P_3E_3)-\frac{1}{2}\varepsilon_b(E_1^2+E_2^2+E_3^2). \quad (5)$$

Under the open-circuit condition, the total electric field is equal to the depolarization field, which can be calculated for a free-charge-absent body by the electrostatic equilibrium equation as $D_{1,1}+D_{2,2}+D_{3,3}=0$.

Due to truncation at the surface of the finite system, the spontaneous polarization is inhomogeneous across the out-of-plane direction. Thus, an additional surface energy is necessary to describe this intrinsic effect. Using the so-called extrapolation length δ_i^{eff},[26,27] the surface energy density is approximately given by

$$f_{\text{surf}} = \frac{D_1^sP_1^2}{2\delta_1^{\text{eff}}}+\frac{D_2^sP_2^2}{2\delta_2^{\text{eff}}}+\frac{D_3^sP_3^2}{2\delta_3^{\text{eff}}}, \quad (6)$$

where D_i^s are the material coefficients related to the gradient energy coefficients and surface orientation.

The temporal evolution of the spontaneous polarization field is described by the time-dependent Ginzburg-Landau (TDGL) equation

$$\frac{\partial P_i}{\partial t} = -M\frac{\delta F}{\delta P_i}, \tag{7}$$

where M is a kinetic coefficient and t is time.

In the following, we consider $PbTiO_3$ nanofilm-dot systems with (001) oriented nanofilm and epitaxial nanodots as shown in Fig. 1(a). The simulation cell is chosen to include a nanodot and a sufficient large region of nanofilm. A two-dimensional (2D) discrete grid is employed with the default element size $\Delta x = \Delta y = 0.4$ nm. We think that the 2D model can capture the features of domain structure in ferroelectrics with a tetragonal ferroelectric phase (e.g., $PbTiO_3$) at suitable conditions. The width and height of the nanodot are l_d and h_d, and those of the nanofilm region are l_f and h_f. The simulation cell is assumed to be periodic along the x direction. To explore the possible formation of VDS, an open-circuit condition is considered by setting $D_\perp = 0$ at the surfaces, with $D_\perp$ being the component of electric displacement perpendicular to the surface. The free surfaces are assumed to be traction-free. A finite element method has been adopted to solve the strain and electric fields.[17] The evolution of polarization is solved numerically by discretizing the TDGL equation in time. At each time step, the strain and electric fields are obtained by solving the mechanical and electrostatic equilibrium equations with the appropriate boundary conditions. Values of the material coefficients[21,24,27,29] in our simulation are listed in Ref. 28.

III. RESULTS AND DISCUSSIONS

A. Formation of domain pattern in ferroelectric nanofilm-dot systems

First of all, we would like to investigate whether a vortex domain pattern can be formed in the nanodot while the nanofilm maintains a polar domain in the region right below the nanodot as indicated in Fig. 1(a). Such a domain pattern is denoted as simple polar-vortex (SPV) pattern. We notice that the nanofilm with sufficiently small thickness tends to form in-plane polar domains under the open-circuit condition. Meanwhile, toroidal domain pattern is favored to form in the nanodot. The geometry and size of the system should play important roles in the appearance of the SPV pattern. Moreover, the ambient temperature, the strain state of the system, as well as external electric field, can affect the domain stability and are also expected to be important in the formation of SPV pattern. In the following, the effects of all these factors, i.e., geometry, size, ambient temperature, external strain, and electric field, would be considered. Specifically, the temperature effect is explored by simulating the system under a cooling-down process, where the temperature gradually decreases to 0 K from a sufficiently high value by a step of 10 K. A random polarization perturbation is used to initiate the simulation at high temperature until the system is not in paraelectric phase. At each temperature, the stable domain pattern is obtained by equilibrating the system for a sufficiently long time.

The domain pattern evolution of a system (i.e., $h_d = l_d = 4$ nm, $h_f = 8$ nm, and $l_f = 20$ nm) during a cooling-down process at zero external strain and electric field is depicted in Fig. 2. To characterize the domain pattern more clearly, in Fig. 2(a) we plot the temperature dependences of the toroidal moment (i.e., $\mathbf{g} = \frac{1}{V}\int_V \mathbf{r} \times \mathbf{P} dV$,[16] with V being the volume of the system and $\mathbf{r}$ the position vector) and the mean polarization of the nanodot region. Note that a domain pattern is likely to be a vortex domain pattern if it appears with a large toroidal moment but small mean polarization. The domain patterns at $T = 300$ K and $T = 250$ K are depicted in Fig. 2(b). From these results, we found that the system undergoes a paraelectric to ferroelectric transition at temperature of about 720 K. Below this transition point, the toroidal moment of the nanodot increases as the temperature decreases, indicating a toroidal domain pattern is formed in the nanodot region. Specifically, at temperature in range of $720\text{ K} > T > 280\text{ K}$, the toroidal moment of the nanodot is nonzero, while the mean polarization maintains a small magnitude along the x direction. From the domain pattern at $T = 300$ K in Fig. 2(b), we can see that the nanofilm-dot system adopts a SPV pattern at this temperature range. The nonzero mean polarization of the vortex domain pattern is due to the fact that the polarization magnitude decreases from the interface to the nanodot region, which leads to a slight asymmetry of the vortex domain pattern. Also due to this reason, the toroidal moment and the x component of the mean polarization are in the same sign. As the temperature decreases to be lower than 280 K, there is a sudden increase

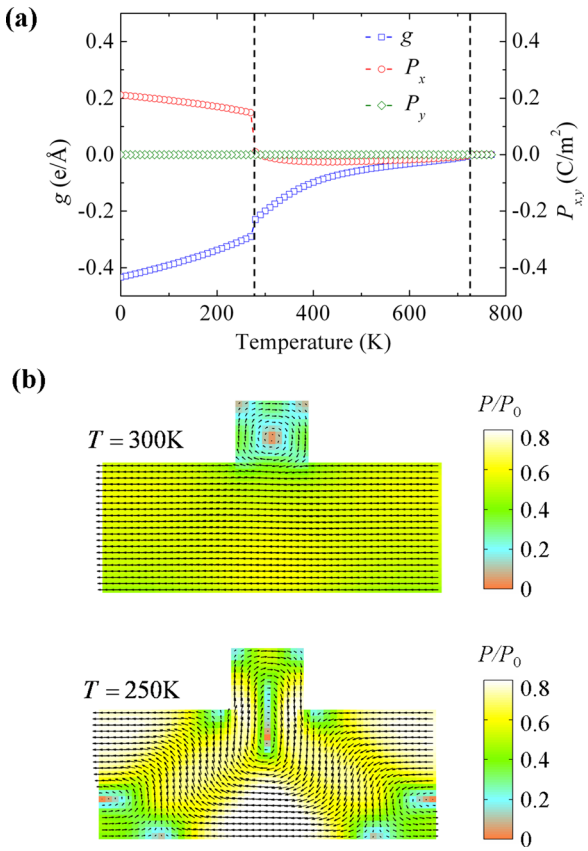

FIG. 2. Domain evolution of a nanofilm-dot system ($h_d = l_d = 4$ nm, $h_f = 8$ nm, and $l_f = 20$ nm) during a cooling-down process at zero external strain and electric field. (a) Toroidal moment and mean polarization as a function of temperature in the nanodot region. (b) The domain patterns at 300 K and 250 K.

of the toroidal moment and the x component of the mean polarization of the nanodot region, and the direction of the mean polarization of the nanodot is also changed, indicating the instability of the SPV pattern. A complex domain pattern is actually formed at this temperature range (see the domain pattern at $T = 250$ K in Fig. 2(b)). In this low temperature range, to avoid the large gradient energy due to the increasing polarization magnitude, the nanodot can not maintain a complete vortex but only a part of it. The vortex extends into the nanofilm region, leading to the formation of a multi-domain pattern with both in-plane and out-of-plane domains in the nanofilm. These results clearly show that the ferroelectric nanofilm-dot system indeed can form SPV pattern, and its stability is a function of temperature.

To see the effect of geometry on the appearance of SPV pattern, in Fig. 3 we further simulate the domain patterns of two nanofilm-dot systems (i.e., $l_d = 4$ nm, $h_f = 8$ nm, and $l_f = 20$ nm) with the height of nanodot being 2 nm and 3.6 nm. Similarly, the two systems are under a cooling-down process at zero external strain and electric field. The temperature dependences of the toroidal moment and the mean polarization of the nanodot region are shown in Figs. 3(a) and 3(b) for the two systems, respectively. The domain patterns at selected temperatures of the two systems are also shown in Figs. 3(c) and 3(d), respectively. Due to their different geometry, the two systems exhibit generally different paths of domain evolution. For the system with the height of nanodot being 2 nm, it does not adopt an apparent SPV pattern during the cooling-down process, although at the very beginning it tends to form such a domain pattern as indicated by the same sign of the toroidal moment and the mean polarization of the nanodot at high temperature. The formation of SPV pattern is suppressed as the toroidal moment gradually changes its sign at temperature of about 350 K after a slight increase in magnitude at high temperature. The nanofilm is found to adopt a polar domain at temperature between 720 K and 170 K. Meanwhile, the nanodot adopts a polarization flux in the same direction of the polar domain of the nanofilm. As the temperature decreases to be lower than 170 K, the nanofilm can not maintain the polar domain but evolves into an asymmetric multi-domain pattern with both in-plane and out-of-plane domains. This transition is accompanied by a jump of the toroidal moment and the mean polarization of the nanodot. Due to the asymmetric domain pattern in the nanofilm, the polarization flux in the nanodot also has a small but nonzero y component. For the system with the nanodot height of 3.6 nm, its domain evolution is quite similar to the one investigated in Fig. 2. It adopts a SPV pattern at a temperature range of $720\,\text{K} > T > 270\,\text{K}$. At lower temperature, SPV pattern becomes instable and transforms into a multi-domain pattern (see Fig. 3(d)).

The domain patterns of other nanofilm-dot systems (i.e., $l_d = 4$ nm, $h_f = 8$ nm, and $l_f = 20$ nm) with the nanodot in height of 1.6 nm to 4 nm at room temperature (i.e., $T = 300$ K)

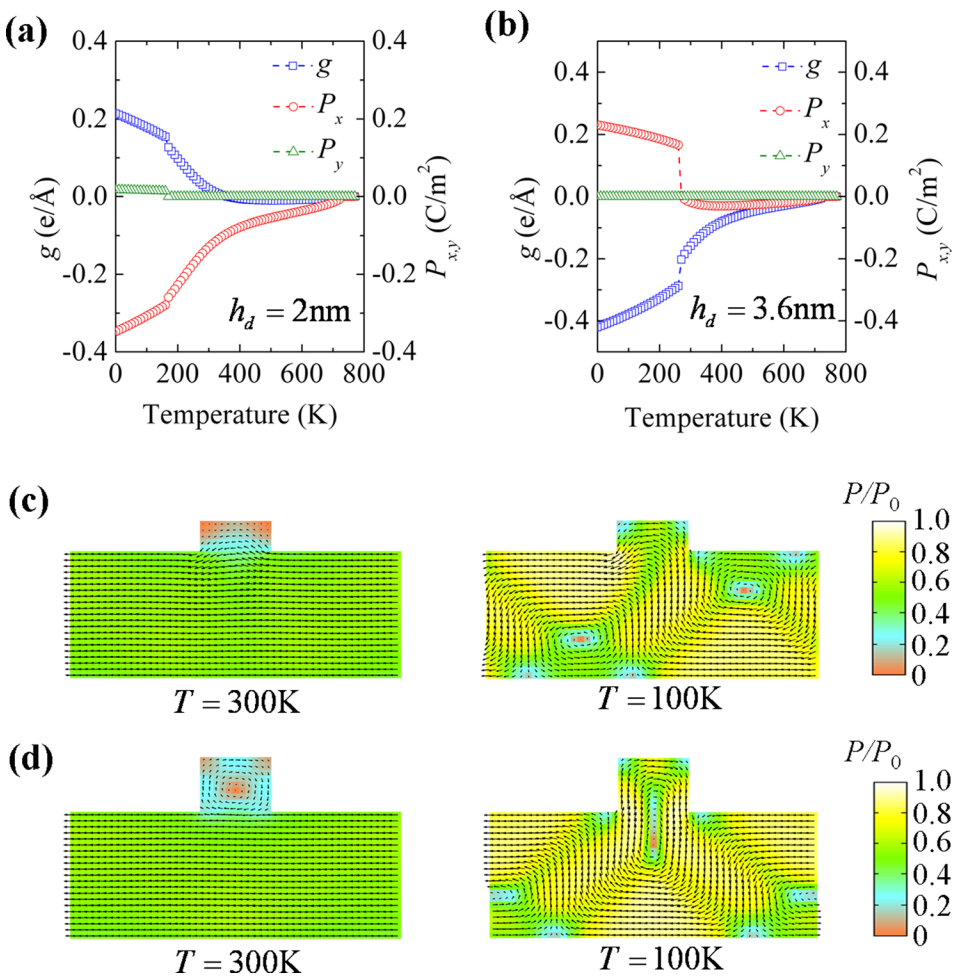

FIG. 3. Domain evolution of two nanofilm-dot systems ($h_d = 4$ nm, $h_f = 8$ nm, and $l_f = 20$ nm) with the height of nanodot being (a) and (c) 2 nm and (b) and (d) 3.6 nm during a cooling-down process at zero external strain and electric field. (a) and (b) Toroidal moment and mean polarization as a function of temperature in the nanodot region. (c) and (d) Domain patterns at 300 K and 100 K.

and free of external fields are simulated to have a deeper insight on the geometry effect. The toroidal moment and the mean polarization of the nanodot region for these systems are depicted in Fig. 4. It can be seen that the toroidal moment and the mean polarization almost linearly depend on the height of nanodot. As the height of nanodot increases from 1.6 nm to 4.0 nm, the toroidal moment of the nanodot changes its sign and increases to a significant magnitude of about 0.2e/Å, whereas the x component of the mean polarization decreases from about 0.17C/m^2 to almost zero, indicating a transition from polar domain pattern to a vortex domain pattern. Specifically, when the height of nanodot is small, i.e., $h_d = 1.6$ nm or 2.0 nm, the toroidal moment of the nanodot is in opposite sign with the x component of the mean polarization of the nanodot. For these systems, SPV pattern is not favored to form and they adopt the domain pattern similar to that shown in Fig. 3(c). The toroidal moment changes its sign as the height of the nanodot reaches 2.4 nm. The system adopts an apparent SPV pattern when the height of the nanodot is larger than 2.8 nm. This result clearly demonstrates the geometry effect on the appearance of SPV pattern.

As the size of the nanofilm-dot system should also has an effect on the domain formation, we further simulate the domain pattern of a system with a larger size (i.e., $h_d = l_d = 6$ nm, $h_f = 12$ nm, and $l_f = 30$ nm). This system has the same geometry of the previously investigated one in Fig. 2, but its size is 1.5 times larger than the previous one. The domain pattern evolution of such a system under cooling-down process at zero external strain and electric field is depicted in Fig. 5. It can be seen that the new system exhibits similar domain evolution path with the previous one, i.e., adopting SPV pattern at a high temperature range and a complex domain pattern at a lower temperature range. However, compared with the previous one, the stable temperature range of SPV pattern of the new system is much narrower (i.e., $730\,\text{K} > T > 580\,\text{K}$). Therefore, the size of the system is indeed important to the appearance of SPV pattern in the nanofilm-dot system. We notice that an in-plane polar domain in the nanofilm right below the nanodot is crucial for the appearance of a complete vortex in the nanodot. As thinner nanofilm is more favored to form in-plane polar domains under the open-circuit condition, systems with thinner nanofilm thus exhibit a wider stable temperature range of SPV pattern.

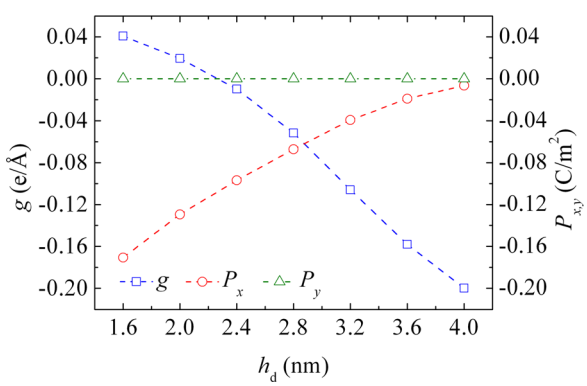

FIG. 4. Toroidal moment and mean polarization in the nanodot region of nanofilm-dot systems ($l_d = 4$ nm, $h_f = 8$ nm, and $l_f = 20$ nm) with the nanodot in height of 1.6 nm–4 nm at room temperature under zero external strain and electric field.

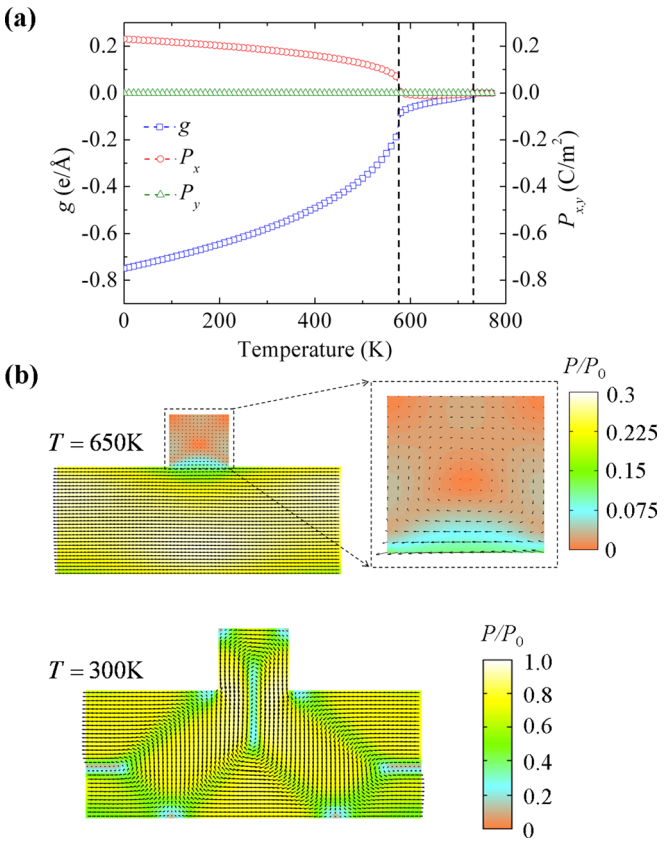

FIG. 5. Domain evolution of a nanofilm-dot system ($h_d = l_d = 6$ nm, $h_f = 12$ nm, and $l_f = 30$ nm) during a cooling-down process at zero external strain and electric field. (a) Toroidal moment and mean polarization as a function of temperature in the nanodot region. (b) Domain patterns at 650 K and 300 K.

It is also well-known that nanofilm tends to form in-plane domains when it is subjected to in-plane tensile strain. Therefore, we believe that SPV pattern should be favored at tensile strain. In contrast, it should be unstable at compressive in-plane strain. To verify this, we further simulate the effect of external in-plane strain ε_{11}^a on domain pattern of the nanofilm-dot system previously investigated in Fig. 2. The evolution of domain patterns during a cooling-down process under a compressive strain $\varepsilon_{11}^a = -0.01$ and a tensile strain $\varepsilon_{11}^a = 0.01$ are depicted in Fig. 6. Result shows that the strain state of the nanofilm-dot system indeed affects the appearing of SPV pattern. As expected, we found that the system does not adopt SPV pattern at $\varepsilon_{11}^a = -0.01$ during the whole cooling-down process (see Figs. 6(a) and 6(c)). In contrast, the system always adopts a SPV pattern at $\varepsilon_{11}^a = 0.01$ during the cooling-down process (see Figs. 6(b) and 6(d)). The ferroelectric transition temperature is also strongly tuned by the external strain. It can be seen from Figs. 6(a) and 6(b) that a compressive strain $\varepsilon_{11}^a = -0.01$ decreases the ferroelectric transition temperature of the nanofilm-dot system to be about 440 K, meanwhile the tensile strain $\varepsilon_{11}^a = 0.01$ increases the ferroelectric transition temperature of the system to be about 1010 K.

It would be also interesting to investigate the effect of external electric field on the stability of SPV pattern in the

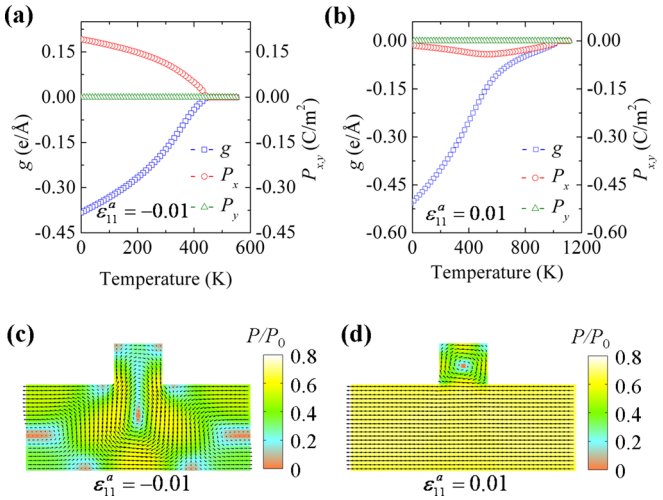

FIG. 6. Domain evolution of a nanofilm-dot system ($h_d = l_d = 4$ nm, $h_f = 8$ nm, and $l_f = 20$ nm) during a cooling-down process under (a) and (c) a compressive strain $\varepsilon_{11}^a = -0.01$ and (b) and (d) a tensile strain $\varepsilon_{11}^a = 0.01$. (a) and (b) Toroidal moment and mean polarization as a function of temperature in the nanodot region. (c) and (d) Domain patterns at 300 K. The system is free of external electric field.

nanofilm-dot system. It is expected that an external electric field along x-direction in the nanofilm region can maintain the in-plane polar domain in the nanofilm and thus stabilize the SPV pattern of the nanofilm-dot system at lower temperature. To see this, we perform a further simulation on the domain evolution of nanofilm-dot system during cooling-down process with different external electric field E_a applied in the nanofilm. The simulated result of a system ($h_d = l_d = 6$ nm, $h_f = 12$ nm, and $l_f = 30$ nm) at free of external strain is depicted in Fig. 7, with the case of $E_a = -5 \times 10^7$ V/m and $E_a = -10^8$ V/m, respectively, shown in Figs. 7(a) and 7(b). Such a system has been previously shown to have a narrow temperature range ($730\,\text{K} > T > 580\,\text{K}$) of stable SPV pattern (see Fig. 5). It can be seen that the SPV pattern indeed can be stabilized by external electric field, manifested with a

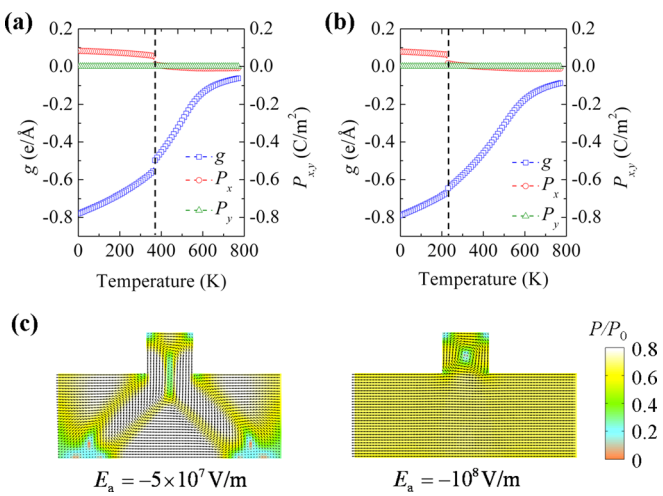

FIG. 7. Domain evolution of a nanofilm-dot system ($h_d = l_d = 6$ nm, $h_f = 12$ nm, and $l_f = 30$ nm) during a cooling-down process with an external electric field (a) $E_a = -5 \times 10^7$ V/m and (b) $E_a = -10^8$ V/m along the x-direction applied in the nanofilm region. (c) Domain patterns at room temperature for the two cases. The system is at zero external strain.

significant increase of the stable temperature range as the electric field increases. For the system under $E_a = -5 \times 10^7$ V/m, the lowest temperature of stable SPV pattern is about 370 K, which is about 200 K lower than the system under zero external electric field (see Figs. 5(a) and 7(a)). Application of an external electric field $E_a = -10^8$ V/m further decreases the lowest temperature of stable SPV pattern to be about 230 K (Fig. 7(b)). The enhanced stability of SPV pattern is also seen from the domain pattern of the system under different external electric field at room temperature (see Fig. 7(c)). Summarizing the results of Figs. 2–7, we can see that SPV pattern can be stabilized in nanofilm-dot systems with suitable size and geometry, meanwhile the stability of SPV pattern is a strong function of ambient temperature, strain state, and external electric field.

B. Switching of vortex domain pattern in a ferroelectric nanofilm-dot system

Finally, after demonstrating the existence of SPV pattern in nanofilm-dot systems, we conduct a simulation to show an alternative strategy for controlling the chirality of vortex domain pattern. Such a strategy utilizes the feature of SPV pattern: the nanodot tends to adopt a vortex domain pattern with the bottom polarization parallel to the polar domain of the nanofilm. In the simulation, the system has an initial stable SPV pattern with a clockwise vortex domain pattern in the nanodot. We apply an electric field of 10^8 V/m in the nanofilm region to reverse polar domain. The simulation domain pattern evolution of a system ($h_d = l_d = 4$ nm, $h_f = 8$ nm, and $l_f = 20$ nm) at room temperature and zero external strain is shown in Fig. 8(a). To see the domain pattern clearer, in Fig. 8(b) we also depict the corresponding domain patterns in the nanodot region. We can see that during the evolution the system first evolves into an intermediate state, where the vortex extends into the nanofilm region. The domain pattern at this state is similar to the previous predicted complex domain pattern (e.g., the domain pattern at $T = 250$ K shown in Fig. 2(b)). The in-plane domains in parallel to the electric field then gradually grow up. As the polar domain is totally reversed, an anticlockwise vortex begins to form in the nanodot. This result clearly shows that the vortex domain pattern in the nanodot can be switched by reversing the adjacent polar domain in the nanofilm.

C. Discussion

We notice that the domain structure of real three-dimensional (3D) nanofilm-dot system would be different from that of simulated 2D system. It is more complicated in 3D system since in-plane vortex domain pattern may form in the nanodot, which can not be captured by our simple 2D simulation. For 3D nanodots that are free-standing or on a paraelectric substrate, an in-plane vortex domain pattern tends to form when the height of the nanodot is small compared with its other two lengths. Such a domain pattern is resulted from the decrease of system's depolarization energy and vortex domain wall energy. For nanofilm-dot system, the formation of domain structure is more complex due to existence of domain coupling across the nanofilm-dot interface. For this case, interfacial domain wall energy plays an

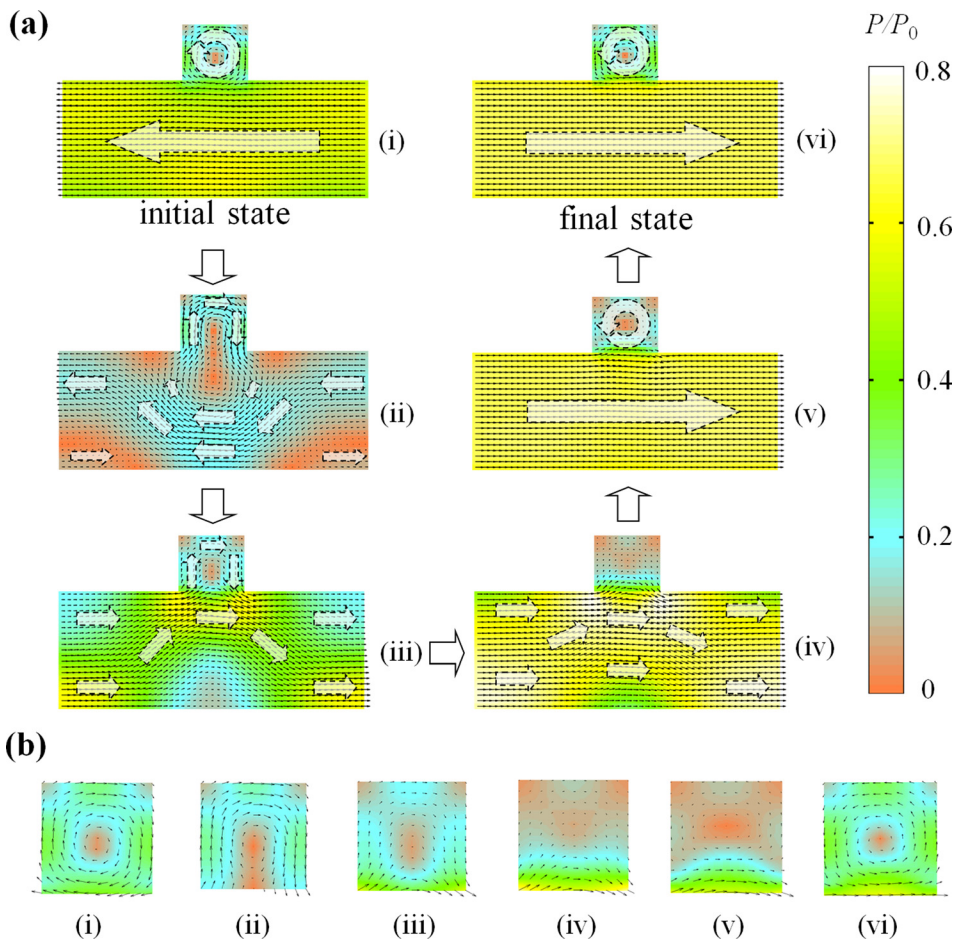

FIG. 8. (a) Domain evolution of a nanofilm-dot system ($h_d = l_d = 4$ nm, $h_f = 8$ nm, and $l_f = 20$ nm) during a process of switching the vortex domain pattern in the nanodot by reversing the polar domain in the nanofilm, and (b) corresponding domain patterns in the nanodot region. The system is at room temperature and zero external strain, and an electric field $E_a = 10^8$ V/m is applied in the nanofilm region.

important role in domain formation of the nanodot. We believe that the mechanism that a decrease of the interfacial domain wall energy helps stabilize a vertical vortex domain pattern in the nanodot is not limited to the simulated 2D configuration. The SPV pattern predicted by our 2D simulation should be also found in 3D nanofilm-dot systems at suitable conditions (e.g., geometry, size, temperature, external strain, and electric field as what we have shown). Nevertheless, for the exact stability dependence of SPV pattern on these conditions in real 3D nanofilm-dot systems, further 3D simulations would be necessary.

IV. CONCLUSIONS

In summary, we have conducted a phase field study on the domain structure in ferroelectric nanofilm-dot systems with a coherent interface between the nanofilm and the nanodot. With taking into account the effects of geometry and size, as well as ambient temperature, external strain, and electric field, our simulations demonstrate that the nanodot can adopt a stable vortex domain pattern, while the nanofilm maintains a polar domain at suitable conditions. We further conduct a simulation to show that the switching of the vortex domain pattern in the nanodot can be achieved by reversing the adjacent polar domain in the nanofilm. Our study proposes an alternative mechanism for controlling the chirality of vortex domain pattern in ferroelectric nanostructures by exploiting the coupling of different types of domain structures.

ACKNOWLEDGMENTS

The authors acknowledge the financial support of the National Natural Science Foundation of China (NSFC) (Nos. 51172291, 11232015, and 11372361). Yue Zheng also thanks support by the Fundamental Research Funds for the Central Universities, NCET in University, Research Fund for the Doctoral Program of Higher Education, Fok Ying Tung Foundation, Science and Technology Innovation Project of Guangdong Provincial Education Department and Guangdong Natural Science Funds for Distinguished Young Scholar.

[1]H. Fu and L. Bellaiche, Phys. Rev. Lett. **91**, 257601 (2003).
[2]I. I. Naumov, L. Bellaiche, and H. Fu, Nature **432**, 737 (2004).
[3]J. F. Scott, Nature Mater. **4**, 13 (2005).
[4]B. J. Rodriguez, X. S. Gao, L. F. Liu, W. Lee, I. I. Naumov, A. M. Bratkovsky, D. Hesse, and M. Alexe, Nano Lett. **9**, 1127 (2009).
[5]A. Schilling, D. Byrne, G. Catalan, K. G. Webber, Y. A. Genenko, G. S. Wu, J. F. Scott, and J. M. Gregg, Nano Lett. **9**, 3359 (2009).
[6]S. Prosandeev and L. Bellaiche, Phys. Rev. B **75**, 094102 (2007).
[7]S. Prosandeev, I. Ponomareva, I. Naumov, I. Kornev, and L. Bellaiche, J. Phys.: Condens. Matter **20**, 193201 (2008).
[8]G. Catalan, J. Seidel, R. Ramesh, and J. F. Scott, Rev. Mod. Phys. **84**, 119 (2012).
[9]I. Ponomareva, I. I. Naumov, and L. Bellaiche, Phys. Rev. B. **72**, 214118 (2005).
[10]S. Prosandeev, I. Ponomareva, I. Kornev, I. Naumov, and L. Bellaiche, Phys. Rev. Lett. **96**, 237601 (2006).
[11]I. Naumov and H. Fu, Phys. Rev. Lett. **98**, 077603 (2007).
[12]S. Prosandeev, I. Ponomareva, I. Kornev, and L. Bellaiche, Phys. Rev. Lett. **100**, 047201 (2008).
[13]S. Prosandeev and L. Bellaiche, Phys. Rev. Lett. **101**, 097203 (2008).

[14]I. Naumov and H. Fu, Phys. Rev. Lett. **101**, 197601 (2008).
[15]J. Wang and M. Kamlah, Phys. Rev. B **80**, 012101 (2009).
[16]W. J. Chen, Y. Zheng, and B. Wang, Appl. Phys. Lett. **100**, 062901 (2012).
[17]W. J. Chen, Y. Zheng, and B. Wang, Sci. Rep. **2**, 796 (2012).
[18]W. J. Chen, Y. Zheng, B. Wang, D. C. Ma, and F. R. Ling, Phys. Chem. Chem. Phys. **15**, 7277 (2013).
[19]X. Fu, I. I. Naumov, and H. Fu, Nano Lett. **13**, 491 (2013).
[20]C. M. Wu, W. J. Chen, Y. Zheng, D. C. Ma, B. Wang, J. Y. Liu, and C. H. Woo, Sci. Rep. **4**, 3946 (2014).
[21]Y. Zheng and C. H. Woo, Appl. Phys. A: Mater. Sci. Process. **97**, 617 (2009); C. H. Woo and Y. Zheng, *ibid.* **91**, 59 (2008).
[22]A. K. Tagantsev, Ferroelectrics **375**, 19 (2008).
[23]M. J. Haun, E. Furman, S. J. Jang, H. A. McKinstry, and L. E. Cross, J. Appl. Phys. **62**, 3331 (1987).
[24]N. A. Pertsev, A. G. Zembilgotov, and A. K. Tagantsev, Phys. Rev. Lett. **80**, 1988 (1998).
[25]L. D. Landau, E. M. Lifshitz, and L. P. Pitaevskii, *Electrodynamics of Continuous Media* (Oxford University Press, Oxford, 1984).
[26]R. Kretschmer and K. Binder, Phys. Rev. B **20**, 1065 (1979).
[27]K. Ishikawa and T. Uemori, Phys. Rev. B **60**, 11841 (1999).
[28]Values of parameters in calculation (SI units and T in K): $a_1 = 3.85(T - 752) \times 10^5$, $a_{11} = -7.3 \times 10^7$, $a_{12} = 7.5 \times 10^8$, $a_{111} = 2.6 \times 10^8$, $a_{112} = 6.1 \times 10^8$, $a_{123} = -3.7 \times 10^9$, $c_{11} = 1.746 \times 10^{11}$, $c_{12} = 0.7937 \times 10^{11}$, $c_{44} = 1.1111 \times 10^{11}$, $Q_{11} = 0.089$, $Q_{12} = -0.026$, $Q_{44} = 0.0675$, $G_{11} = 2G_{44} = 2G'_{44} = 2G_{110}$, $G_{110} = 1.73 \times 10^{-10}$, $\delta_i^{\text{eff}} = 5 \times 10^{-9}$, $\varepsilon_b = 4.425 \times 10^{-10}$, and $P_0 = 0.757$.
[29]Y. L. Li, S. Y. Hu, Z. K. Liu, and L. Q. Chen, Appl. Phys. Lett. **81**, 427 (2002).